ACS APPLIED MATERIALS & INTERFACES

Research Article

www.acsami.org

Effects of Adsorbed F, OH, and Cl Ions on Formaldehyde Adsorption Performance and Mechanism of Anatase TiO_2 Nanosheets with Exposed {001} Facets

Peng Zhou,[†] Xiaofeng Zhu,[†] Jiaguo Yu,*[,†] and Wei Xiao*[,‡]

[†]State Key Laboratory of Advanced Technology for Material Synthesis and Processing, Wuhan University of Technology, Luoshi Road 122#, Wuhan 430070, P.R. China

[‡]School of Resource & Environmental Sciences, Wuhan University, Wuhan, 430072, P.R. China

Supporting Information

ABSTRACT: Formaldehyde (HCHO), as the main indoor air pollutant, is highly needed to be removed by adsorption or catalytic oxidation from the indoor air. Herein, the F^-, OH^-, and Cl^--modified anatase TiO_2 nanosheets (TNS) with exposed {001} facets were prepared by a simple hydrothermal and post-treatment method, and their HCHO adsorption performance and mechanism were investigated by the experimental analysis and theoretical simulations. Our results indicated that the adsorbed F^-, OH^-, and Cl^- ions all could weaken the interaction between the HCHO and TNS surface, leading to the serious reduction of HCHO adsorption performance of TNS. However, different from F^- and Cl^- ions, OH^- ion could induce the dissociative adsorption of HCHO by capturing one H atom from HCHO, resulting in the formation of one formyl group and one H_2O-like group. This greatly reduced the total energy of the HCHO adsorption system. Thus, the adsorbed OH^- ions could provide the additional active centers for HCHO adsorption. As a result, the NaOH-treated TNS showed the best HCHO adsorption performance mainly because its surface F^- was replaced by OH^-. This study will provide new insight into the design and fabrication of high performance adsorbents for removing indoor HCHO and, also, will enhance the understanding of the HCHO adsorption mechanism.

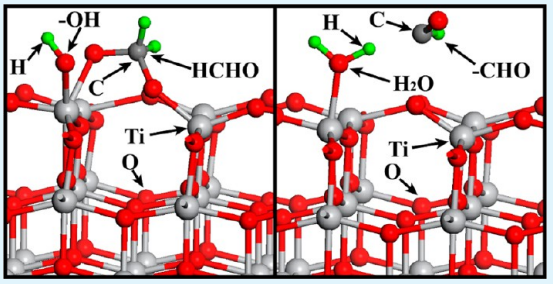

KEYWORDS: *TiO_2 nanosheets, formaldehyde, adsorption performance, F ions, hydroxyl group, dissociative adsorption*

1. INTRODUCTION

Formaldehyde (HCHO), a colorless and pungent-smelling gas, is considered as the main indoor air pollutant in modern houses, mainly released from building materials and spray-painted furniture.[1] It is well-known that HCHO can easily combine with proteins, which increases the risks of asthma, allergy, nausea, edema, dyspnea, and other symptoms. Therefore, it is quite necessary to develop sensitive and practical materials for removing HCHO from air, which has attracted enormous attentions from both academic and industrial communities. As a result, a lot of materials, such as TiO_2,[2−6] SiO_2,[7−9] $Ni(OH)_3$,[8] SnO_2,[10] Fe_2O_3,[2,9] ZnO,[3] WO_3,[4] RuO_2,[5] V_2O_5,[6] and corresponding composites, have been investigated on addressing the HCHO concern. Among them, TiO_2 is considered as the suitable material for the adsorption, detection, and decomposition of HCHO, owing to its chemical stability, biocompatibility, rich source, long lifetime, and low cost.[11−17] It is worth noting that the reconstruction of the TiO_2 surface induced by the HCHO adsorption is the foundation of HCHO detection.[18] In addition, the HCHO adsorption on the TiO_2 surface is the first step of HCHO decomposition.[13] Hence, the HCHO adsorption performance of TiO_2 indirectly determines the detection and decomposition of HCHO. Thus it is highly desirable to clarify the adsorption mechanism of HCHO and further improve the HCHO adsorption performance of TiO_2. The related theory calculations revealed that compared to the thermodynamically stable anatase {101} surface and rutile {110} of TiO_2, the anatase {001} surface of TiO_2 exhibited the higher activity for HCHO adsorption due to its unusual surface structure and chemistry.[19−21] Consequently, the {001} surface of anatase TiO_2 has the potential application for developing the high-performance HCHO adsorbent. Fortunately, the anatase TiO_2 nanosheets (TNS) with exposed {001} facets and large specific surface area have been successfully synthesized and applied to the environmental protection.[22−29] Therefore, TNS can be used as the ideal materials for HCHO adsorption. However, during usual synthesis and treatments of TNS, some prevalent ions, such as F^-, OH^-, and Cl^-, tend to be adsorbed on the TNS surface, which has been verified by many investigations.[23,30−32] Therefore, the most obtained TNS surfaces are polluted by these ions. As a result, the surface chemistry environment of

Received: June 9, 2013
Accepted: August 5, 2013
Published: August 5, 2013

   dx.doi.org/10.1021/am402246b | ACS Appl. Mater. Interfaces 2013, 5, 8165−8172

TNS will be changed by those introduced foreign ions, leading to the variation of HCHO adsorption performance of TNS. Furthermore, another possibility can not be neglected that the adsorbed ions can directly combine with HCHO, regardless of the TNS surface status. Thus, the HCHO adsorption on the F^-, OH^-, and Cl^--adsorbed TNS surface needs to be investigated, which is beneficial to clearly understand the favorable/unfavorable factors for HCHO adsorption and further improve the HCHO adsorption performance of TNS. But to the best of our knowledge, such an issue remains unexplored yet.

Herein, the HCHO adsorption on the F^-, OH^-, and Cl^--adsorbed TNS surface is investigated by experimental and theoretical methods, for the first time. It is found that the NaOH-treated TNS exhibits the best HCHO adsorption performance. Such experimental results are explained and correlated in line with the theoretical simulations regarding the geometry structures, electron density difference plots (EDDP), and adsorption energies (E_{ads}) of the various HCHO adsorption models. This study will provide some new insight into optimizing TiO_2 for HCHO adsorption.

2. EXPERIMENTAL AND COMPUTATIONAL SECTION

2.1. Preparation. The anatase TiO_2 nanosheets were synthesized by a hydrothermal method using tetrabutyl titanate and HF solution as precursors.[23,29] Briefly, 3 mL of 40 wt % HF solution was added into 25 mL of tetrabutyl titanate liquid dropwise under magnetic stirring for 30 min. Then, the obtained mixture was transferred into a 50 mL Teflon-lined autoclave and kept at 180 °C for 24 h. After reaction, the Teflon-lined autoclave was naturally cooled to room temperature, the white precipitates were collected by centrifuging and then washed with distilled water and ethanol for five times, respectively. Finally, the washed precipitates were dried in an oven at 70 °C for 12 h. The obtained products were labeled as HF-TNS. Afterward, 2 g of HF-TNS was dispersed in the 150 mL of 1 mol L^{-1} NaOH solution under 30-min magnetic stirring. Then, the precipitates were collected again and washed with distilled water five times. Similarly, the precipitates were dried in an oven at 70 °C for 12 h. The obtained products were notated as NaOH-TNS. Moreover, 1 g of NaOH-TNS was added into 50 mL of 1 mol L^{-1} HCl solution. The above washing and drying processes were repeated. The obtained products were represented as HCl-TNS.

2.2. Characterization. The X-ray diffraction (XRD) patterns, obtained on an X-ray diffractometer (Rigaku, Japan) using Cu Kα radiation at a scan rate of 0.05° 2θ s^{-1}, were used to characterize the crystalline phase of the samples. The accelerating voltage and applied current were 40 kV and 80 mA, respectively. Transmission electron microscopy (TEM) and high-resolution transmission electron microscopy (HRTEM) analysis were conducted by a JEM-2100F electron microscope (JEOL, Japan) with a 200 kV accelerating voltage. The morphology of samples was obtained from an S-4800 field emission scanning electron microscopy (FESEM) (Hitachi, Japan) at an acceleration voltage of 20 kV. The Brunauer–Emmett–Teller (BET) specific surface area (S_{BET}) of the samples was analyzed in a nitrogen adsorption apparatus (Micromeritics ASAP 2020, USA). Before nitrogen adsorption measurements, all the as-prepared samples were degassed at 180 °C. The BET surface area was determined by a multipoint BET method using adsorption data in the relative pressure (P/P_0) range of 0.05–0.3. The pore-size distributions were determined by the nitrogen adsorption volume via the Barret–Joyner–Halender (BJH) method assuming a cylindrical pore model. The nitrogen adsorption volume at a relative pressure (P/P_0) of 0.972 was used to calculate the pore volume and the average pore size. X-ray photoelectron spectroscopy (XPS) measurements were done in a VG ESCALAB 210 electron spectrometer with Mg Kα (1253.6 eV) source and a multichannel detector. All the binding energies were referenced to the C 1s peaks at 284.8 eV from adventitious carbon.

2.3. HCHO Adsorption Test. The HCHO adsorption performance of HF-TNS, NaOH-TNS, and HCl-TNS was measured in an organic glass box equipped with a 5-W fan under room temperature (25 °C). A 0.3 g portion of the adsorbent was coated on the bottom of a glass Petri dish with a diameter of 14 cm. Then the sample-coated dish was covered by a piece of glass slide and placed in the bottom of the reactor. Afterward, 10 μL of condensed HCHO (38%) was injected into the reactor. After 2–3 h, the HCHO solution was completely volatilized and the concentration of HCHO became stabilized. Concentrations of gaseous HCHO were online analyzed by using a Photoacoustic IR Multigas Monitor (INNOVA air Tech Instruments Model 1412). The HCHO vapor was allowed to reach an adsorption/desorption equilibrium within the reactor prior to the experiments. The initial concentration of HCHO in equilibrium was controlled at about 167 ppm, which remained constant until the glass-slide cover on the Petri dish was removed to trigger HCHO adsorption. The decreased concentrations of HCHO were used to evaluate the HCHO adsorption performance of the samples.

2.4. Computational Details. As an effective method to study the molecular adsorption on the surface of solid oxide, the density-functional-theory (DFT) calculation was used to analyze the HCHO adsorption on TNS surface. All DFT calculations were performed by the CASTEP package based on the plane-wave-pseudopotential approach.[33] Considering the relatively small atomic numbers of elements in the current system, the Perdew–Burke–Ernzerhof (PBE) of the generalized gradient approximation (GGA) was used as the exchange-correlation function.[34,35] The interaction between valence electrons and the ionic core was described by the ultrasoft pseudopotential. Before building the model of TNS surface, the unit cell of anatase TiO_2 was optimized using the cutoff energy of 400 eV and the Monkhorst–Pack k-point mesh of 4 × 4 × 4.[36] The obtained structure parameters are a = 3.807 Å and c = 9.667 Å, which is very consistent with the previous experimental and theoretical investigations.[37−40] This indicated the reliability of current calculations. Considering that the TNS is mainly with exposed {001} facets, four repeating {001} trilayer (O–Ti–O) units were used to simulate the TNS surface. The interaction between adjacent atom slabs was eliminated by the vacuum slab with thickness of 15 Å.

To eliminate the interaction between adjacent HCHO molecules, the 2 × 2 supercell (0.25 ML) was introduced to simulate the HCHO adsorption system, which was proved to be successful in characterizing the current adsorption system according to the previous investigation.[19] The cutoff energy of 400 eV and the Monkhorst–Pack k-point mesh of 4 × 4 × 1 were adopted to conduct the geometry optimization calculations. The tolerances of energy, force, stress, and displacement in the optimized calculation were 2.0 × 10^{-5} eV per atom, 0.05 eV $Å^{-1}$, 0.1 GPa, and 0.002 Å, respectively. During the optimized calculation, the positions of all atoms were optimized except for those in the bottom trilayer of the atom slab. Moreover, the more trilayer units, the thicker the vacuum slab,

the higher the cutoff energy, the larger the supercell, and the wider the Monkhorst–Pack *k*-point mesh, respectively. The obtained results suggested that the variations were smaller than 0.001 Å in displacement and 0.002 eV in energy, indicating high accuracy of present calculations. The optimized model of TNS surface was shown in Figure S1 of the Supporting Information (SI). It can be clearly seen that the O_{2C} atoms are exposed in the outermost layer and the Ti_{5C} atoms constitute the second atomic layer. Simultaneously, a surface energy (E_S) of 1.04 eV was obtained, which was calculated by the following formula:[41]

$$E_S = (E_{slab} - E_{bulk})/2A$$

where E_{slab} is the total energy of 2 × 2 supercell (containing 16 Ti atoms and 32 O atoms) of the TNS surface, E_{bulk} is the total energy of the 2 × 2 × 1 supercell (also containing 16 Ti atoms and 32 O atoms) of bulk TiO_2, and 2*A* is the contacting area between the atomic slab and vacuum slab. The result is similar to one recent report using the PBE of GGA,[19] which authenticated the reliability of current calculations. The geometry optimization calculations of HCHO adsorption systems follow the above parameter settings. After the geometry optimization calculations, the EDDP and total energies of simulated adsorption system were calculated.

3. RESULTS AND DISCUSSION

3.1. Phase Structure and Morphology. XRD patterns of the as-prepared absorbents (HF-TNS, NaOH-TNS, and HCl-TNS) are presented in Supporting Information Figure S2. It is observed that all peaks are well indexed with the anatase TiO_2 (JPCDS 21-1272). No other diffraction peaks are observed, indicating high purity of the samples. The TEM image of the HF-TNS (see Figure 1) displays the predominant existence of

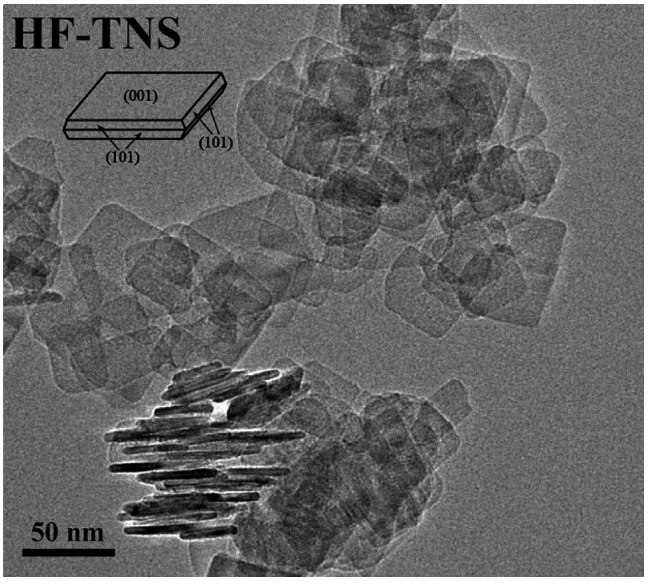

Figure 1. TEM image of the HF-TNS sample.

nanosheet-shaped structures. On the basis of the calculation method in the previous literature,[23] the percentage of {001} facets in the HF-TNS is estimated to be about 90% on average. Similar to the HF-TNS, the NaOH-TNS and HCl-TNS samples also exhibit pure anatase TiO_2 and the sheet-shaped structures (see Supporting Information Figure S2 and S3). Besides, the FESEM images of the HF-TNS, NaOH-TNS, and HCl-TNS samples are given in Supporting Information Figure S4, which also verify the existence of sheet-shaped structures. All the XRD patterns, TEM and FESEM images are consistent with those reported results regarding anatase TNS with exposed {001} facets.[22,23] Therefore, all the as-obtained samples are anatase TNS with exposed {001} facets, as schematically illustrated in the inset of Figure 1. It is also suggested that the phase and microstructures of TNS remains unchanged upon washing in either NaOH or HCl solutions.

Nitrogen adsorption–desorption isotherms and corresponding pore-size distribution curves of the as-prepared absorbents are shown in Supporting Information Figure S5. The isotherms of the absorbents all have the obvious hysteresis loops at high relative pressure between 0.8 and 1.0, which is defined as type IV mesoporous solids according to the Brunauer–Deming–Deming–Teller (BDDT) classification.[42] The pore sizes of as-prepared absorbents share the same distribution ranging from 5 to 25 nm (see the inset of Figure S5). Moreover, the shapes of these hysteresis loops all agree with the type of H3, indicating the existences of narrow slit-shaped pores associated with sheet-like morphology. This is well consistent with the results of TEM. It should be noted that the adsorption–desorption isotherms of NaOH-TNS and HCl-TNS shift downward slightly compared to that of HF-TNS, implying a slight decrease of BET surface area. This is due to the fact that a small percentage of pores are filled with the sediments during washing with NaOH or HCl solutions. But the specific surface areas and pore-size distributions of the HF-TNS, NaOH-TNS, and HCl-TNS are still comparable.

3.2. XPS and Surface Analysis. Figure 2 shows the high-resolution XPS spectra of the HF-TNS, NaOH-TNS, and HCl-

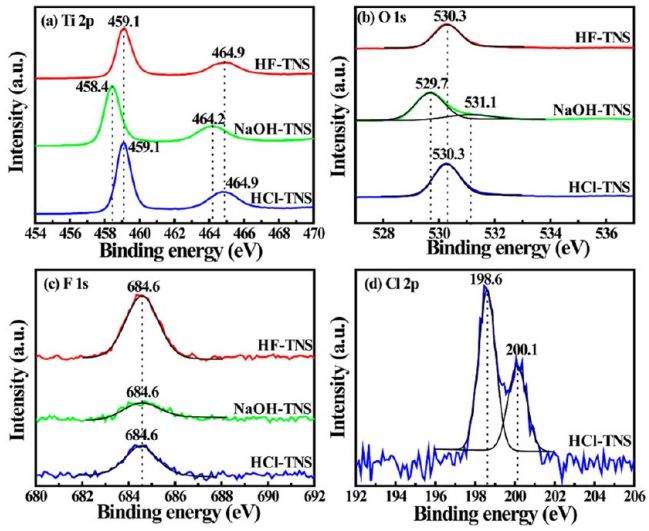

Figure 2. High-resolution XPS spectra of Ti 2p (a), O 1s (b), F 1s (c), and Cl 2p (d) regions for the HF-TNS, NaOH-TNS, and HCl-TNS samples.

TNS. It is shown in Figure 2a and b that the peaks of Ti $2p_{3/2}$, Ti $2p_{1/2}$, and O 1s in the HF-TNS and HCl-TNS occur at 459.1, 464.9, and 530.3 eV, respectively.[22,25−28] However, the peaks of Ti $2p_{3/2}$, Ti $2p_{1/2}$, and O 1s in the NaOH-TNS all shift downward to 458.4, 464.2, and 529.7 eV, implying that the Ti and O atoms in the NaOH-TNS possess more electrons than those in the HF-TNS and HCl-TNS. In addition, a relatively weak shoulder peak appears at 531.1 eV in the O 1s spectrum

dx.doi.org/10.1021/am402246b | ACS Appl. Mater. Interfaces 2013, 5, 8165−8172

of the NaOH-TNS, assigned to the adsorbed OH^- ions (hydroxyl groups).[43] Such a peak is absent in the O1s spectra of the HF-TNS and HCl-TNS, indicating that the hydroxyl groups only exist on the NaOH-TNS surface. Furthermore, the F 1s XPS spectra of HF-TNS, NaOH-TNS, and HCl-TNS all exhibit the peak (684.6 eV) of surface fluoride (≡Ti—F) (see Figure 2c).[22] In addition, the peak (688.5 eV) of lattice F atom is not found, implying that all present F are the adsorbed F atoms.[23] However, the difference is that the intensities of F 1s peaks in the XPS spectra of both NaOH-TNS and HCl-TNS are obviously lower than that of HF-TNS. The peaks of Cl $2p_{3/2}$ (198.6 eV) and Cl $2p_{1/2}$ (200.1 eV) only appear in the XPS spectra of the HCl-TNS.[43,44]

To investigate the variation in the quantities of elements during NaOH or HCl treatments, Table 1 summarizes the

Table 1. Atomic Ratios of Ti, O_L, O_H, F, and Cl for the HF-TNS, NaOH-TNS, and HCl-TNS Samples[a]

sample	Ti	O_L	O_H	F	Cl
HF-TNS	1.00	2.29	0	0.37	0
NaOH-TNS	1.00	2.04	0.57	0.13	0
HCl-TNS	1.00	2.32	0	0.15	0.06

[a] O_L and O_H represent the O atoms in the lattice of TiO_2 and the hydroxyl group, respectively.

atomic ratio of Ti, O_L (the lattice O atom), O_H (the O atom in hydroxyl groups), F, and Cl in the HF-TNS, NaOH-TNS, and HCl-TNS. For the convenience of discussion, the atomic ratio of Ti was assumed to be unity. It is suggested that a large number of hydroxyl groups are adsorbed on the NaOH-TNS surface. However, the atomic ratio of F decreases from 0.37 in the HF-TNS to 0.13 in the NaOH-TNS, suggesting that NaOH treatment promotes the substitution of the adsorbed F^- ions by the OH^- ions from the NaOH solution. But the partial F^- still adsorbs on the NaOH-TNS surface due to the strong interaction between F^- ions and TNS surface. Besides, the disappearance of hydroxyl groups in the HCl-TNS indicates that HCl treatment can effectively eliminate the adsorbed hydroxyl groups on TNS surface. But the atomic ratio of F in HCl-TNS is approximately consistent with that in NaOH-TNS, implying that the F^- ions are also not removed by the HCl treatment. Simultaneously, Cl^- ions from HCl solution are introduced onto the TNS surface. The obvious difference in quantities between F and Cl are derived from the relatively weaker interaction between Cl^- ion and TNS surface.

To further interpret the results of XPS measurements and investigate the reconstructions of TNS surfaces induced by the adsorbed F^-, OH^-, and Cl^- ions, the geometry structure models of F^-, OH^-, and Cl^--adsorbed TNS surface are calculated by the DFT theory. F^-, OH^-, and Cl^- ions are deliberately introduced onto the surface of TNS with exposed {001} facets, and the corresponding F^--, OH^--, and Cl^--adsorbed {001} surfaces are simulated. The partial optimized structures and corresponding EDDP are shown in Figure 3. It can be clearly seen that the F^- (see Figure 3b1), OH^- (see Figure 3c1), and Cl^- (see Figure 3d1) ions all tend to be bonded to the Ti_{5C} atoms in the TNS surface. Meanwhile, the corresponding Ti_{5C} atoms tend to move outward. But the newly formed Ti_{5C}—F (1.79 Å) and Ti_{5C}—O_H (1.83 Å) bonds are more stable than the newly formed Ti_{5C}—Cl (2.32 Å) bond, due to the larger electronegativity of F and O than that of Cl.

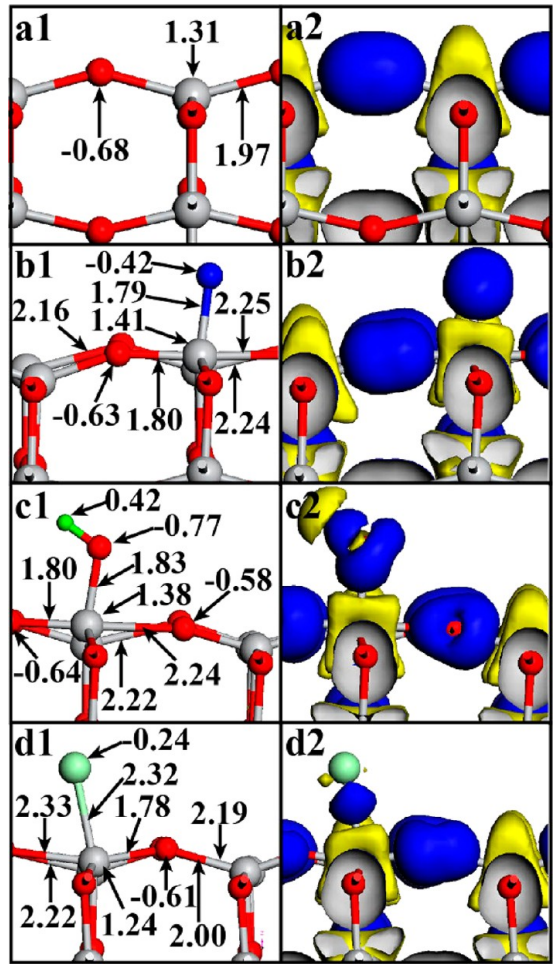

Figure 3. Partial optimized geometry structures and corresponding electron density difference plots: clean {001} surface (a), F^--adsorbed {001} surface (b), OH^--adsorbed {001} surface (c), Cl^--adsorbed {001} surface (d). The isosurfaces of electron density difference plots all are 0.05 e/Å^3. The numbers pointing to atoms stand for the Mulliken populations of atoms and the numbers pointing to bonds stand for the lengths (Å) of bonds. The blue and red surfaces represent charge accumulation and depletion, respectively. The blue sphere stands for the F atom, the green one, for the H atom, and the pale green one, for Cl atom.

As can be seen from the corresponding EDDP, the F^--adsorbed {001} surface (see Figure 3b2) and OH-adsorbed {001} surface (see Figure 3c2) exhibit the strong chemisorptions of F^- and OH^- ions on the TNS surface, while the Cl^--adsorbed {001} surface (see Figure 3d2) shows the relatively weak chemisorption of Cl^- ions on the TNS surface. The stronger chemisorptions of F^- and OH^- ions than that of Cl^- on the TNS surface are in good accordance with the observed higher atomic ratios of O_H and F than that of Cl (see Table 1) in the samples. Moreover, the slightly shorter length of Ti_{5C}—F (1.79 Å) than that of Ti_{5C}—O_H (1.83 Å) means that the preadsorbed F^- ions on the TNS surface are difficult to be completely replaced by the OH^- ions. The above EDDP also implies the redistribution of charges in the TNS surface.

As an effective parameter to characterize the charge of an atom, the Mulliken population is used to analyze the charge transfer in the TNS surface. The Mulliken populations of Ti_{5C} atoms bonded to F^- and OH^- ions are 1.41 (Figure 3b1) and 1.38 (Figure 3c1), respectively, which explain the difference

between the binding energies of Ti $2p_{3/2}$ (Ti $2p_{1/2}$) in the XPS spectra (Figure 2a) of HF-TNS and NaOH-TNS. However, the Mulliken population of the Ti_{5C} atom bonded to Cl^- ion decreases to 1.24 (Figure 3d1), lower than that of the Ti_{5C} atom in the clean TNS surface (1.31, see Figure 3a1). This is because the Cl^- ion not only forms a weak Ti_{5C}–Cl bond (2.32 Å) but also significantly weakens one of two adjacent Ti_{5C}–O_{2C} bonds (2.33 and 1.78 Å, see Figure 3d1). Such effects lead to the reductions of Ti_{5C} atoms. But the reduced Ti_{5C} atoms are too few to be detected by XPS due to the small quantity of adsorbed Cl^- ions (Table 1). Besides, the atomic ratio of F is higher than that of Cl in the HCl-TNS (see Table 1), resulting in the domination of F^- ions instead of Cl^- ions. Thus, the binding energy of Ti $2p_{3/2}$ (Ti $2p_{1/2}$) in the HCl-TNS is consistent with that in the HF-TNS (Figure 2a). Similarly, though the adsorbed F^- ions also exist on the NaOH-TNS surface, the quantity of adsorbed OH^- ions is larger than that of F^- ions. Therefore, the binding energy of Ti 2p in the HF-TNS and HCl-TNS both are higher than that in the NaOH-TNS.

Moreover, the formation of the strong Ti_{5C}–F bonds in the F^- and Cl^--adsorbed {001} surfaces remarkably weakens the adjacent Ti_{5C}–O_{2C} bonds, which then prevents the electrons of the Ti_{5C} atoms transferring to the O_{2C} atoms. In comparison with the Ti_{5C}–F bonds, the Ti_{5C}–O_H bonds in the OH^--adsorbed {001} surface are slightly weak. Hence, the O_{2C} atoms adjacent to the adsorbed OH^- ions possess more electrons than those adjacent to the adsorbed F^- ions. As a result, the binding energies of O 1s in the HF-TNS and HCl-TNS are larger than that in the NaOH-TNS, which agrees well with the XPS results. Besides, the extended Ti_{5C}–O_{2C} bonds are easier to be broken owing to the weakened binding force, which is beneficial to the HCHO adsorption.

3.3. Evaluation of HCHO Adsorption Performance. Figure 4 shows the comparison of HCHO adsorption performance for the HF-TNS, NaOH-TNS, and HCl-TNS samples. It is suggested in Figure 4 that the HCHO adsorption performance for the three samples decreases in an order of NaOH-TNS > HCl-TNS > HF-TNS. To explain the difference in the HCHO adsorption performances of HF-TNS, NaOH-TNS, and HCl-TNS, the HCHO adsorptions on the F^-, OH^-, and Cl^--adsorbed {001} surfaces are simulated and calculated by DFT. For comparison, the HCHO adsorption on clean {001} surface is also considered. It should be noted that the absolutely clean {001} surface is difficult to prepare. Hence, the HCHO adsorption on the clean {001} surface is only investigated by the theoretical method.

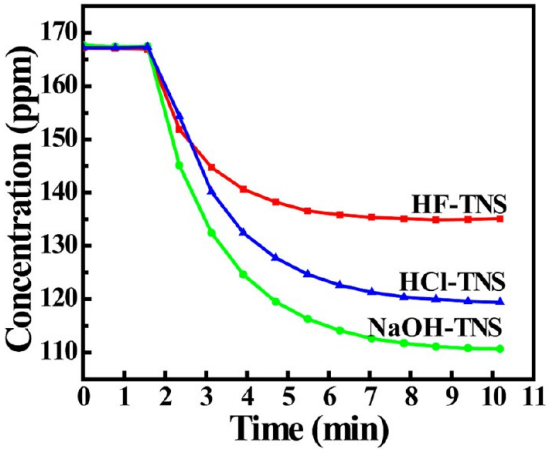

Figure 4. Comparison of formaldehyde adsorption performance for the HF-TNS, NaOH-TNS, and HCl-TNS samples.

According to the atomic configuration in the {001} surface, two models (types I and II) of the HCHO adsorption on the {001} surface are calculated. The optimized geometry structures and corresponding EDDP are shown in Figure 5.

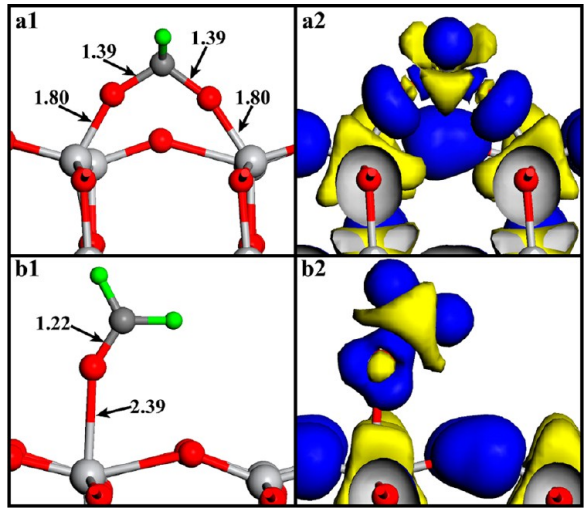

Figure 5. Partial optimized geometry structures and corresponding electron density difference plots: type I (a) and type II (b).

In type I (see Figure 5a1), the C atom and O_F atoms in the formaldehyde molecule are respectively bonded to one O_{2C} atom and one Ti_{5C} atom due to the break of corresponding Ti_{5C}–O_{2C} bond. As a result, the structure of Ti–O–C–O–Ti linkage is formed in the {001} surface. Further, the EDDP (see Figure 5a2) of type I also exhibits the strong chemisorption of HCHO on the {001} surface. Also, the newly formed Ti_{5C}–O_F bond (1.80 Å) and the adjacent Ti_{5C}–O_{2C} bond (1.80 Å) are shorter than the Ti_{5C}–O_{2C} bonds (1.97 Å, see Figure 3a1) in the clean {001} surface, indicating that the HCHO adsorption enhances the structural stability of the {001} surface. However, in type II (see Figure 5b1), the O_F atom is directly bonded to the Ti_{5C} atom, but the C atom from HCHO is not bonded to any atoms from TNS. As a result, the adjacent Ti_{5C}–O_{2C} bonds are not broken. Besides, the newly formed Ti_{5C}–O_F bond (2.39 Å) is longer than that (1.80 Å) in type I, indicating the weaker interaction between HCHO and {001} surface in type II. Moreover, the EDDP (see Figure 5b2) of type II also exhibits the weak chemisorption of HCHO on the {001} surface. Further investigation reveals that the adsorption energy (E_{ads}) of type I (2.48 eV) is much larger than that of type II (0.78 eV), which is calculated by the following formula:[19,41]

$$E_{ads} = E_{slab} + E_{HCHO} - E_{total}$$

where E_{slab} is the energy of {001} surface, E_{HCHO} is the energy of one HCHO molecule in the vacuum, and E_{total} is the total energy of HCHO-adsorbed {001} surface. This suggests that type I is more stable than type II, implying that type I is the favorable mode of HCHO adsorption on the {001} surface. Thus, type I is discussed in the following investigation on HCHO adsorption on the F^-, OH^-, and Cl^--adsorbed {001} surfaces, and type II is skipped.

The above analysis on the F^-, OH^-, and Cl^--adsorbed {001} surfaces suggests that the adsorbed F^-, OH^-, and Cl^- ions lead

dx.doi.org/10.1021/am402246b | ACS Appl. Mater. Interfaces 2013, 5, 8165–8172

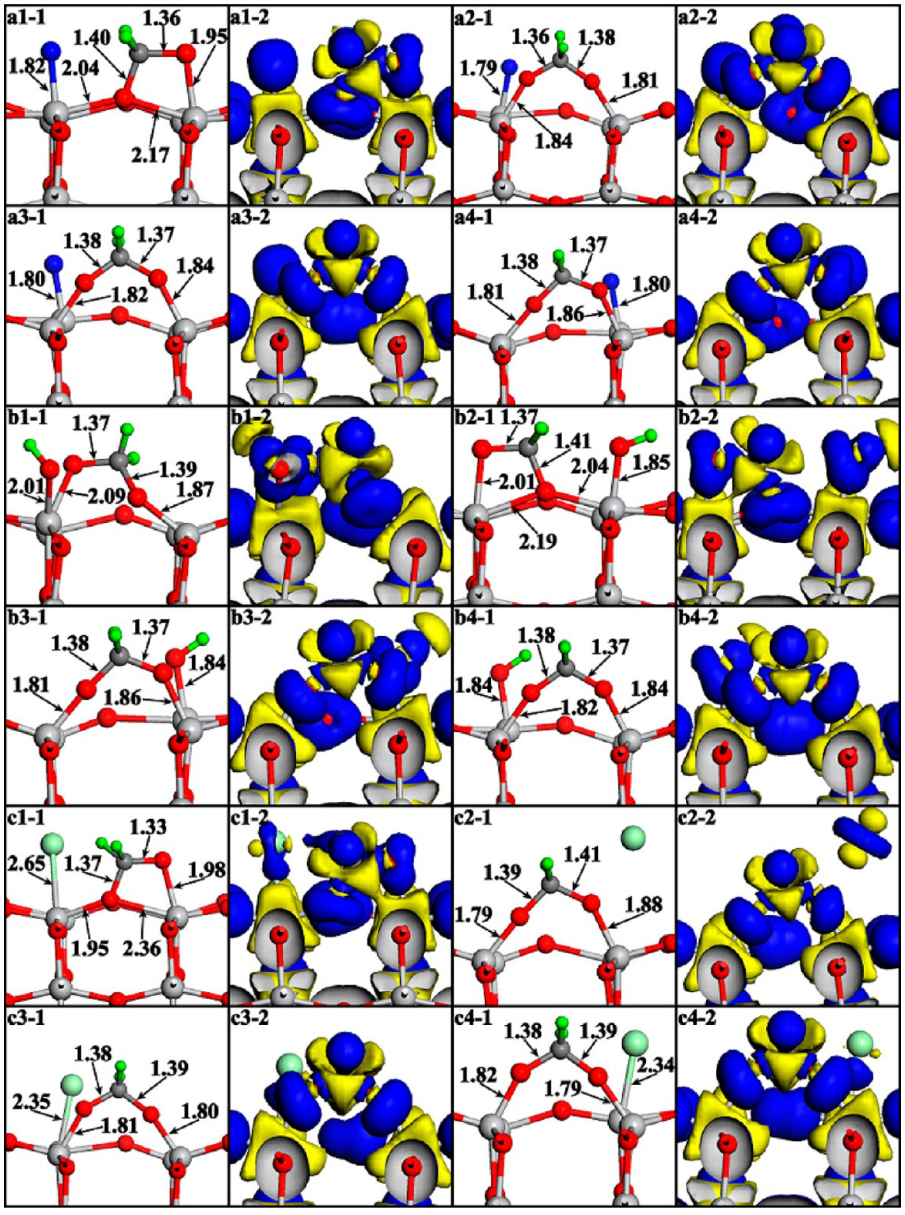

Figure 6. Partial optimized geometry structures and corresponding electron density difference plots: HCHO adsorptions on F^--adsorbed {001} surface (a1, a2, a3, and a4), OH^--adsorbed {001} surface (b1, b2, b3, and b4) and Cl^--adsorbed {001} surface (c1, c2, c3, and c4).

Table 2. E_{ads} of HCHO adsorptions on F^-, OH^-, and Cl^--Adsorbed {001} Surface for Type I

surface		E_{ads} (eV)	surface		E_{ads} (eV)	surface		E_{ads} (eV)
	a1	1.31		b1	0.84		c1	1.47
F^--adsorbed	a2	1.74	OH^--adsorbed	b2	1.48	Cl^--adsorbed	c2	0.96
{001}	a3	1.84	{001}	b3	1.90	{001}	c3	2.00
	a4	1.80		b4	1.85		c4	2.02

to the extension of partial $Ti_{5C}-O_{2C}$ bonds. Considering the characteristic of type I, the weakened $Ti_{5C}-O_{2C}$ bonds are easier to be broken during HCHO adsorption. Thus the four longest $Ti_{5C}-O_{2C}$ bonds in each of F^-, OH^-, and Cl^--adsorbed {001} surfaces are investigated on the HCHO adsorption. As can be seen in Figure 6, the HCHO molecules are all chemisorbed on the F^-, OH^-, and Cl^--adsorbed {001} surfaces via the mode of type I. But the difference is that some $Ti_{5C}-O_{2C}$ bonds (see Figure 6a1, 6b2, and 6c1) are not broken. The occurrence of unbroken $Ti_{5C}-O_{2C}$ bonds is ascribed to the difficulties for the O_{2C} atoms moving outside owing to the strong repulsive forces from the adjacent F^-, OH^-, and Cl^- ions. As a result, the O_{2C} atom bonded to the C atom of HCHO is still close to the Ti_{5C} atom boned to the O_F atom, which stabilizes the $Ti_{5C}-O_{2C}$ bond. Though the O_{2C} atom is adjacent to the adsorbed OH^- ion (see Figure 6b1), the $Ti_{5C}-O_{2C}$ bond is still broken. This is due to the deflection of OH^- ion, which decreases the repulsive force between the O_{2C} atom and the OH^- ion.

dx.doi.org/10.1021/am402246b | ACS Appl. Mater. Interfaces 2013, 5, 8165−8172

Moreover, the $Ti_{5C}-O_{2C}$ bond with the O_{2C} atom adjacent to the Cl^- ion is also broken (see Figure 6c2). This is due to the desorption of the Cl^- ion, which weakens the repulsive force between the O_{2C} atom and Cl^- ion. Hence, the additional interactions between the O_H atoms and the adsorbed ions (F^-, OH^-, and Cl^-) improve the total energies of adsorption systems, which significantly decreases the E_{ads} of HCHO adsorption systems (see Table 2). But the adsorption systems with the HCHO far away from the adsorbed ions have the larger E_{ads} than those with the HCHO close to the adsorbed ions. This implies that the adsorbed F^-, OH^-, and Cl^- ions retard the HCHO adsorption on the {001} surface. Moreover, it can be concluded that HCHO prefers to be adsorbed on the clean {001} surface rather than the F^-, OH^-, and Cl^--adsorbed {001} surfaces via type I mode. But according to Table 2, the HCHO adsorption on the Cl^--adsorbed {001} surfaces has the larger E_{ads} than those on the F^- and OH^--adsorbed {001} surfaces. In addition, the adsorbed ions in HCl-TNS are less than those in HF-TNS and NaOH-TNS. As a result, HCl-TNS should have the best HCHO adsorption performance. But the above experimental investigation confirms that NaOH-TNS has better HCHO adsorption performance than HCl-TNS. This implies the existence of other effective adsorption mode of HCHO on the {001} surface of TiO_2.

It is well-known that the F^- ion and the O_H atom with lone electron pairs can form hydrogen bonds with H atoms. Thus, it is possible that the adsorbed ions (F^-, OH^-, and Cl^-) can directly combine with HCHO, also resulting in the HCHO adsorption. Accordingly, the interactions (type III) between HCHO and adsorbed ions (F^-, OH^-, and Cl^-) are investigated (see Figures 7a, c, and d). Besides, considering the O_F atom with lone electron pairs in HCHO molecules, the interaction between the H_H atom (the H atom in hydroxyl) and the O_F atom is also explored (see Figure 7b). Surprisingly, as HCHO is close to the adsorbed OH^- ion, the C_F-H_F bond in HCHO is broken, and then, the H_F is bonded to the O_H atom (see Figure 7c1). Thus, one formyl group and one H_2O-like group are formed, which is similar to the previous report.[45] Though the EDDP suggests that the interaction between the two groups is the weak physisorption (see Figure 7c2), the current adsorption system has the much larger E_{ads} (0.97 eV) than the HCHO adsorption on the F^- and Cl^--adsorbed {001} surface (see Table 3). This indicates that the transferring of H_F atom from HCHO to the adsorbed OH^- ion is beneficial to the HCHO adsorption on the {001} surface. But the H_H atom from OH^- is not attracted by the O_F atom (see Figure 7b1 and 7b2), leading to the low E_{ads} (0.20 eV). Such a phenomenon does not appear in the F^- and Cl^--adsorbed {001} surfaces (see Figure 7a and d). Furthermore, the above XPS results confirm that a large number of OH^- ions are adsorbed on the NaOH-TNS surface. Hence, the OH^--adsorbed {001} surface has more active centers for HCHO adsorption than the F^- and Cl^--adsorbed {001} surfaces. It is not surprising that NaOH-TNS exhibits the best HCHO adsorption performance. Moreover, our recent results indicate that the HCHO decomposition using Pt-loaded TiO_2 as catalyst is also enhanced by NaOH treatment.[46] This is because the formed formyl group induced by the adsorbed OH^- ions has a positive influence on the HCHO decomposition.

4. CONCLUSIONS

In summary, the F^- ions from HF, OH^- ions from NaOH, and Cl^- ions from HCl all can be chemisorbed on the {001} surfaces of TNS, resulting in the reconstruction of TNS surface. The adsorbed ions (F^-, OH^-, and Cl^-) directly weaken the interactions between the HCHO molecules and the $Ti_{5C}-O_{2C}$ bonds in the {001} surfaces, which significantly reduces the E_{ads} of HCHO adsorption systems. However, different from the adsorbed F^- and Cl^- ions, the adsorbed OH^- ion can easily capture the H_F atom from the HCHO molecule, which significantly reduces the total energy of HCHO adsorption system. As a result, the adsorbed OH^- ion produces the extra active centers for HCHO adsorption. Thus the NaOH-treated TNS exhibit enhanced HCHO adsorption performance. Moreover, the formed formyl and H_2O-like groups on NaOH-TNS will enhance the adsorption and decomposition of formaldehyde. This study will provide new insight into the

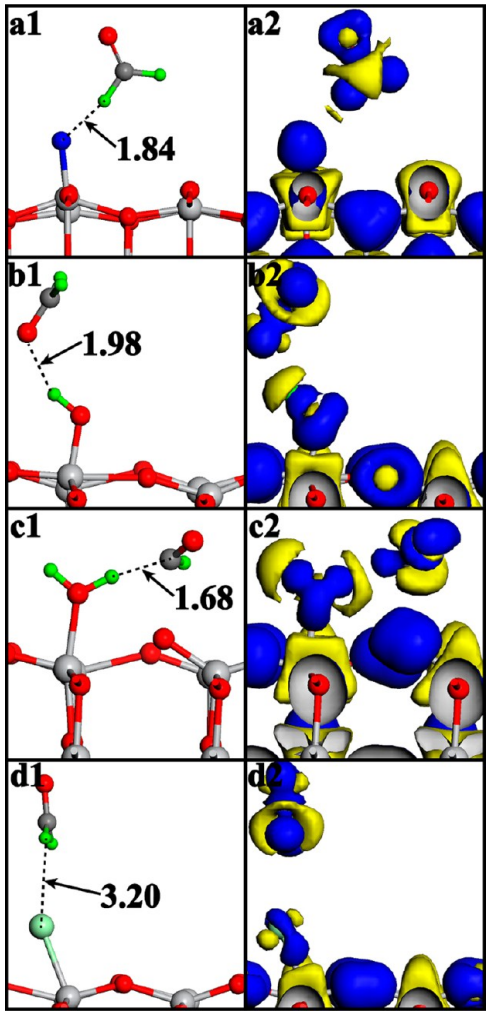

Figure 7. Partial optimized geometry structures and corresponding electron density difference plots: HCHO adsorptions on F^--adsorbed {001} surface (a), OH^--adsorbed {001} surface (b and c), and Cl^--adsorbed {001} surface (d).

Table 3. E_{ads} of HCHO Adsorptions on F^-, OH^-, and Cl^--Adsorbed {001} Surface for Type III

	surface	E_{ads} (eV)
a	F^--adsorbed {001}	0.03
b	OH^--adsorbed {001}	0.20
c	OH^--adsorbed {001}	0.97
d	Cl^--adsorbed {001}	0.23

dx.doi.org/10.1021/am402246b | ACS Appl. Mater. Interfaces 2013, 5, 8165−8172

understanding of HCHO adsorption mechanism on the surface of oxides.

■ ASSOCIATED CONTENT

Supporting Information

Additional figures and details (PDF). This material is available free of charge via the Internet at http://pubs.acs.org.

■ AUTHOR INFORMATION

Corresponding Author

*Tel.: 0086-27-87871029. Fax: 0086-27-87879468. E-mail: jiaguoyu@yahoo.com (J.Y.). Tel./Fax: 86-27-68775799. E-mail: gabrielxiao@whu.edu.cn (W.X.).

Notes

The authors declare no competing financial interest.

■ ACKNOWLEDGMENTS

This work was partially supported by the 863 Program (2012AA062701), 973 program (2013CB632402), and NSFC (51072154, 21177100, and 51272199). Also, this work was financially supported by the Fundamental Research Funds for the Central Universities (2013-VII-030) and Self-determined and Innovative Research Funds of SKLWUT (2013-ZD-1).

■ REFERENCES

(1) Collins, J. J.; Ness, R.; Tyl, R. W.; Krivanek, N.; Esmen, N. A.; Hall, T. A. *Regul. Toxicol. Pharmacol.* **2001**, *34*, 17−34.
(2) Yang, J. J.; Li, D. X.; Zhang, Z. J.; Li, Q. L.; Wang, H. Q. *J. Photochem. Photobio. A* **2000**, *137*, 197−202.
(3) Liao, Y. C.; Xie, C. S.; Liu, Y.; Chen, H.; Li, H. Y.; Wu, J. *Ceram. Int.* **2012**, *38*, 4437−4444.
(4) Kim, J.; Kay, B. D.; Dohnálek, Z. *J. Phys. Chem. C* **2010**, *114*, 17017−17022.
(5) Fukunaga, M. T.; Guimares, J. R.; Bertazzoli, R. *Chem. Eng. J.* **2008**, *136*, 236−241.
(6) Akbarzadeh, R.; Umbarkar, S. B.; Sonawane, R. S.; Takle, S.; Dongare, M. K. *Appl. Catal., A* **2010**, *374*, 103−109.
(7) Le, Y.; Guo, D. P.; Cheng, B.; Yu, J. G. *Appl. Surf. Sci.* **2013**, *274*, 110−116.
(8) Xu, Z. H.; Yu, J. G.; Liu, G.; Cheng, B.; Zhou, P.; Li, X. Y. *Dalton Trans.* **2013**, *42*, 10190−10197.
(9) Xu, Z. H.; Yu, J. G.; Xiao, W. *Chem.—Eur. J.* **2013**, *19*, 9592−9598.
(10) Wang, J.; Liu, L.; Cong, S. Y.; Qi, J. Q.; Xu, B. K. *Sensor. Actuat. B* **2008**, *134*, 1010−1015.
(11) Noguchi, T.; Fujishima, A. *Environ. Sci. Technol.* **1998**, *32*, 3831−3833.
(12) Shang, J.; Xie, S. D.; Zhu, T.; Li, J. *Environ. Sci. Technol.* **2007**, *41*, 7876−7880.
(13) Raskó, J.; Kecskés, T.; Kiss, J. *J. Catal.* **2004**, *226*, 183−191.
(14) Zhang, C. B.; Liu, F. D.; Zhai, Y. P.; Ariga, H.; Yi, N.; Liu, Y. C.; Asakura, K.; Flytzani-Stephanopoulos, M.; He, H. *Angew. Chem., Int. Ed.* **2012**, *51*, 9628−9632.
(15) Zhang, C. B.; He, H.; Tanaka, K. *Appl. Catal., B* **2006**, *65*, 37−43.
(16) Huang, H. B.; Leung, D. Y. C. *ACS Catal.* **2011**, *1*, 348−354.
(17) Tan, C.; Fan, W. H.; Wang, W. X. *Environ. Sci. Technol.* **2012**, *46*, 469−476.
(18) Chen, H.; Liu, Y.; Xie, C.; Wu, J.; Zeng, D.; Liao, Y. *Ceram. Interfaces* **2012**, *38*, 503−509.
(19) Liu, H. Z.; Wang, X.; Pan, C. X.; Liew, K. M. *J. Phys. Chem. C* **2012**, *116*, 8044−8053.
(20) Liu, H.; Zhao, M.; Lei, Y.; Pan, C.; Xiao, W. *Comput. Mater. Sci.* **2012**, *51*, 389−395.
(21) Haubrich, J.; Kaxiras, E.; Friend, C. M. *Chem.-Eur. J* **2011**, *17*, 4496−4506.
(22) Sun, L.; Zhao, Z. L.; Zhou, Y. C.; Liu, L. *Nanoscale* **2012**, *4*, 613−620.
(23) Lv, K. L.; Xiang, Q. J.; Yu, J. G. *Appl. Catal., B* **2011**, *104*, 275−281.
(24) Jiang, B. J.; Tian, C. G.; Pan, Q. J.; Jiang, Z.; Wang, J. Q.; Yan, W. S.; Fu, H. G. *J. Phys. Chem. C* **2011**, *115*, 23718−23725.
(25) Yu, J. G.; Dai, G. P.; Xiang, Q. J.; Jaroniec, M. *J. Mater. Chem.* **2011**, *21*, 1049−1057.
(26) Xiang, Q. J.; Yu, J. G.; Jaroniec, M. *Chem. Commun.* **2011**, *47*, 4532−4534.
(27) Xiang, Q. J.; Yu, J. G.; Wang, W. G.; Jaroniec, M. *Chem. Commun.* **2011**, *47*, 6906−6908.
(28) Xiang, Q. J.; Yu, J. G.. *Chin. J. Catal.* **2011**, *32*, 525−531.
(29) Lv, K. L.; Cheng, B.; Yu, J. G.; Liu, G. *Phys. Chem. Chem. Phys.* **2012**, *14*, 5349−5362.
(30) Xiang, Q. J.; Yu, J. G.; Jaroniec, M. *Nanoscale* **2011**, *3*, 3670−3678.
(31) Liuan, G.; Wang, J. Y.; Cheng, H.; Zhao, Y. Z.; Liu, L. F.; Han, X. J. *ACS Appl. Mater. Inter.* **2013**, *5*, 3085−3093.
(32) Liu, G.; Yang, H. G.; Wang, X. W.; Cheng, L.; Pan, J.; Lu, G. Q.; Cheng, H. M. *J. Am. Chem. Soc.* **2009**, *131*, 12868−12869.
(33) Segall, M. D.; Lindan, P. J. D.; Probert, M. J.; Pickard, C. J.; Hasnip, P. J.; Clark, S. J.; Payne, M. C. *J. Phys.-Condens. Mat.* **2002**, *14*, 2717−2744.
(34) Perdew, J. P.; Burke, K.; Ernzerhof, M. *Phys. Rev. Lett.* **1996**, *77*, 3865−3868.
(35) Perdew, J. P.; Wang, Y. *Phys. Rev. B* **1992**, *45*, 13244−13249.
(36) Monkhorst, H. J.; Pack, J. D. *Phys. Rev. B* **1976**, *13*, 5188−5192.
(37) Burdett, J. K.; Hughbanks, T.; Miller, G. J.; Richarson, J. W.; Smith, J. V. *J. Am. Chem. Soc.* **1987**, *109*, 3639−3646.
(38) Zhou, P.; Yu, J. G.; Wang, Y. X. *Appl. Catal., B* **2013**, *142−143*, 45−53.
(39) Yu, J. G.; Zhou, P.; Li, Q. *Phys. Chem. Chem. Phys.* **2013**, *15*, 12040−12047.
(40) Gao, H. T.; Ding, C. H.; Dai, D. M. *J. Mol. Struc.−Theochem* **2010**, *944*, 156−162.
(41) Liu, H. Z.; Zhao, M. T.; Lei, Y. K.; Pan, C. X.; Xiao, W. *Comput. Mater. Sci.* **2012**, *51*, 389−395.
(42) Sing, K. S. W.; Everett, D. H.; Haul, R. A. W.; Moscou, L.; Pierotti, R. A.; Rouquerol, J.; Siemieniewska, T. *Pure Appl. Chem.* **1985**, *57*, 603−619.
(43) Wang, X. K.; Wang, C.; Jiang, W. Q.; Guo, W. L.; Wang, J. G. *Chem. Eng. J.* **2012**, *189*, 288−294.
(44) Cao, Y. Q.; Yu, Y. L.; Zhang, P.; Zhang, L. L.; He, T.; Cao, Y. *Sep. Purif. Technol.* **2013**, *104*, 256−262.
(45) Takahashi, H.; Hori, T.; Wakabayashi, T.; Nitta, T. *J. Phys. Chem. A* **2001**, *105*, 4351−4358.
(46) Nie, L. H.; Yu, J. G.; Li, X. Y.; Cheng, B.; Liu, G.; Jaroniec, M. *Environ. Sci. Technol.* **2013**, *47*, 2777−2783.